



## Research on Terrain Response of the Maintenance Armored Security Vehicle

Quyen DAO MANH<sup>1</sup> , Thang TRAN DUC<sup>2,\*</sup> , Thanh NGUYEN HUY<sup>3</sup> , Duong LE VAN<sup>2</sup> , Dat CHU VAN<sup>2</sup> 

<sup>1</sup>University of Transport Technology, Institute of Mechanical Engineering, 11400, Hanoi, Vietnam

<sup>2</sup>Le Quy Don Technical University, Institute of Vehicle and Energy Engineering, 11900, Hanoi, Vietnam

<sup>3</sup>Le Quy Don Technical University, Faculty of Special Equipment, 11900, Hanoi, Vietnam

### Highlights

- The article focuses on the study of the dynamics of a maintenance armored security vehicle.
- The road excitation is considered the primary influencing factor.
- The research model is unique in that it combines a crane and a truck while moving.

### Article Info

Received: 21 July 2024

Accepted: 24 Dec 2024

### Keywords

Armored vehicles  
Cable  
Dynamic  
Mobile crane  
Rough road

### Abstract

Armored vehicles used for transporting soldiers, integrated with booms and transforming into maintenance armored security vehicles, are a highly effective solution in situations requiring the lifting and movement of heavy objects over short distances. This article presents the dynamics of a maintenance armored security vehicle capable of holding objects while moving on a random rough road or sinusoidal rough road at various speeds. The research model is unique in that it combines a crane and a truck while moving. The 2D dynamic model in this study considers the elasticity of the suspension system, tires, boom cables, and wind load. Random rough road surfaces and the system of differential motion equations are solved using simulation methods in Matlab/Simulink software. The results of the article demonstrate the ability of maintenance armored security vehicles to respond to terrain conditions while simultaneously holding and moving objects on different road surfaces. The findings of the article provide a basis for evaluating the operational capabilities of maintenance armored security vehicles, aiming to propose technical solutions to minimize load oscillations during vehicle movement.

## 1. INTRODUCTION

The goal of developing multifunctional military vehicles, machinery, and equipment is always of interest to the armed forces of various countries. Essentially, these vehicles always perform several primary functions but can, in some situations, assume additional roles through the integration of supplementary equipment. A simple example is an armored personnel carrier whose primary function is to transport infantry on the battlefield but can be integrated with a boom (Figure 1), which, in certain situations, can be used as a crane to transport heavy objects such as engines, tracks, tank wheels, etc. After completing the task, the boom should be able to be detached and installed neatly on the vehicle. In some countries with underdeveloped economies, military equipment is often used for extended periods, prompting a constant need for improvement to enhance effectiveness. The BRDM-2 armored personnel carrier, produced by the Soviet Union since the 1960s, is still in service in the armed forces of many countries, including Vietnam. This vehicle can be integrated with a boom to become a maintenance armored security vehicle (ASV). The boom is hinged to the vehicle's hull and held by cables while lifting and suspending heavy objects, utilizing a chain hoist.

Researching the process by which the ASV both suspends an object and moves over rough road is essential for evaluating the working process and proposing reasonable technical solutions to improve the stability of both the object and the base vehicle during movement. This working process is characterized by several key features:

\*Corresponding author, e-mail: thangdt135@mta.edu.vn

- i) The movement process of the ASV is similar to the characteristics of a two-axle truck moving on randomly uneven or sinusoidal road surfaces, where the vehicle experiences stimuli from the road surface through its tires. Therefore, rough road surfaces greatly affect the oscillation of the object.
- ii) The movement process of the ASV involves suspending the object with chains, subjecting it to the effects of wind loading, while the boom is held with an elastic cable. Therefore, this process shares similarities with the process of lifting a load or lifting the boom of a crawler crane.



**Figure 1.** The maintenance armored security vehicle; a) ASV M1117 b) improved BRDM-2 vehicle

The unique aspect of this research model lies in the combination of the two factors analyzed. The authors have not come across any publications about this model, as most published works focus on individual research, such as stationary cable cranes or two-axle trucks on roads. In the study of vehicle oscillations, the two-axle vehicle model is the most basic. Many studies have investigated the oscillations of two-axle vehicles in a flat or 3D model. These studies typically aim to achieve two main objectives: First, examine the influence of the road surface on the vehicle's oscillations or devices attached to the vehicle body. Second, to propose control strategies to improve ride comfort during vehicle movement, with these control strategies primarily affecting the suspension system.

In [1,2], the authors presented a model of a two-axle vehicle with 7 degrees of freedom moving on a sinusoidal road surface to study the vehicle's response to road stimuli and proposed improving the suspension system from the original linear suspension system to a nonlinear one to minimize the vehicle's vibration caused by the road surface. The 3D model of the two-axle vehicle with 7 degrees of freedom and the influence of a randomly shaped road surface were examined in [3], where the authors investigated the vehicle's oscillations under different conditions of suspension stiffness and vehicle speed. In [4], a 2D model of a two-axle vehicle with load distribution along the vehicle's length and constant speed was considered to evaluate the effects of a random road surface, suspension stiffness, and damping coefficient of the vehicle's axles on the vehicle's oscillations. The analysis of the impact of longitudinal powertrain layout parameters on vehicle and driver oscillations was studied in [5,6]. In [7], the authors focused on researching advanced suspension systems to replace the original suspension system to mitigate vehicle oscillations, increase driver comfort, and improve handling performance for mining vehicles. Similar studies aimed at improving ride smoothness were presented in [8]. Studies on the dynamics of automobiles to propose control solutions affecting the vehicle's suspension system or cabin suspension system were also conducted in documents [9–12]. In the studies on vehicle oscillations mentioned above, all address the roughness of the road surface. The random roughness of the road surface is detailed in documents [13–17]. Studies on the dynamics of wheel cranes, crawler cranes, tower cranes, or gantry cranes during lifting or holding operations related to the elastic deformation of cables have been extensively published. Generally, these studies consider the cable as an elastic element with stiffness and damping coefficients. Some studies disregard the damping coefficient, treating the cable only as an elastic element. In [18–20], the authors presented studies on the dynamics of wheel cranes during stationary operation. In these studies, the cable is considered an elastic element with damping and viscous friction coefficients. Wind loading acting on the lifted load or the lifting boom has been considered during lifting operations and identified as one of the factors influencing the oscillation of the object during equipment operation [18,20]. Studies on the

dynamics of crawler cranes are presented in [21–24]. In these studies, the cable's elasticity affects the equipment's operation, particularly the lifting process, through conversion to an elastic element with a damping coefficient. Cable deformation is considered to have two components: static deformation caused by a static load and dynamic deformation caused by a dynamic load during equipment operation [21,22]. Comparing crawler cranes and wheel cranes, cable deformation is more closely monitored in crawler cranes. To improve the equipment's working efficiency by reducing the oscillation of the boom or the object, the authors also propose control solutions by influencing the drive torque of the lifting mechanism. In studies on the dynamics of tower cranes [25–28] and gantry cranes [29,30], authors have also addressed the elastic deformation of lifting cables. It can be observed that, in these research models, the influence of cable elasticity is significant and directly impacts the stability during the equipment's operation.

The study on the dynamics of ASV during holding objects and movement is significant. The study presented a novel research model, and the results serve as a basis for evaluating the stability of the object during the vehicle's movement. Additionally, it provides a foundation for proposing practical technical solutions to minimize vibration.

## 2. MATERIAL AND METHOD

### 2.1. The Dynamic Model

The dynamic model for studying the oscillation of ASV consists of a working device, which is a boom linked to the chassis of a two-axle vehicle by a hinge joint. The load is suspended by a chain attached to a manually operated pulley block described by a non-elastic rope (Figure 2).

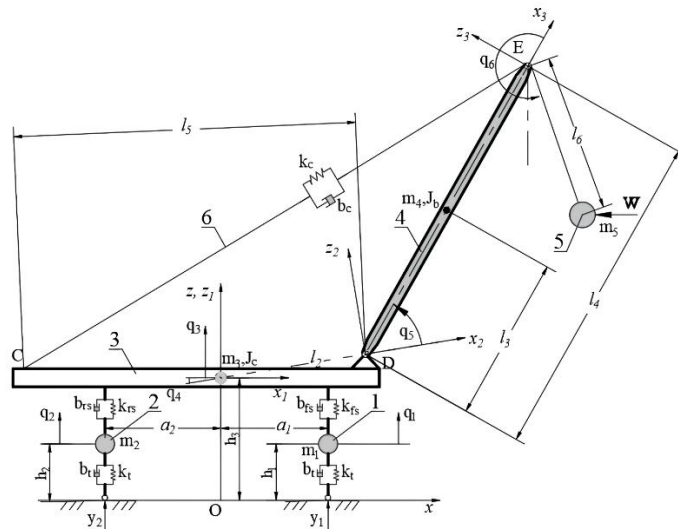


**Figure 2.** Dynamic model of the maintenance armored security vehicle; 1) front axle 2) rear axle 3) vehicle chassis 4) boom 5) object 6) boom cable

The entire system is placed in a fixed coordinate system ( $Oxz$ ) attached to the ground. The considered masses include:  $m_1$  and  $m_2$  are the masses of the front and rear axles, respectively;  $m_3$  is the mass of the vehicle chassis;  $m_4$  is the mass of the boom; and  $m_5$  is the mass of the object. The cable holding the boom is described by an elastic element with stiffness and damping coefficients  $k_c, b_c$ ; the tires have stiffness and damping coefficients  $k_t, b_t$ ; the front suspension system has stiffness and damping coefficients  $k_{fs}, b_{fs}$ ; the rear suspension system has stiffness and damping coefficients  $k_{rs}, b_{rs}$ ; the distances from the center of the vehicle chassis to the center of the front and rear axles, the suspension cable attachment point  $C$ , and the link point  $D$  between the crane and the vehicle chassis in the horizontal direction are  $a_1, a_2, l_1$ , and  $l_2$ , respectively; the distances from  $D$  to the center of the lifting boom and from  $D$  to the suspension cable attachment point  $E$  are  $l_3$  and  $l_4$ , respectively;  $l_5$  is the length of  $CD$ ;  $l_6$  is the length of the object suspension cable;  $J_c, J_b$  are the inertia moments of masses  $m_3$  and  $m_4$ , respectively, with respect to their corresponding rotation axes. During movement, the ASV is subjected to stimuli from a randomly rough or sinusoidal road

characterized by two excitation functions ( $y_1, y_2$ ) and a horizontal wind resistance force ( $W$ ). The extended coordinate vectors to investigate the oscillation of the system consisting of six components (Figure 2) are:

$$\begin{bmatrix} q_1 & q_2 & q_3 & q_4 & q_5 & q_6 \end{bmatrix}^T$$

where  $q_1$  (m),  $q_2$  (m) are the displacements of the center of mass of the front and rear axles of the vehicle chassis, respectively;  $q_3$  (m) is the vertical displacement of the center of mass of the vehicle chassis;  $q_4$  (rad) is the pitch angle of the vehicle chassis;  $q_5$  (rad) is the pitch angle of the crane in the relative coordinate system  $Ox_2z_2$ ; and  $q_6$  (rad) is the pitch angle of the load in the relative coordinate system  $Ox_3z_3$ .

### 2.2. Road Excitation Function and Wind Resistance Force

The rough road surface in related studies is determined using two main methods. Experimental methods offer high accuracy but are costly. Therefore, many studies have utilized simulation methods based on the ISO 8068 standard [13–17]. According to this standard, the rough road surface is divided into eight classes. Through simulation methods, the roughness profile of the road surface can be described as a function of road length [13–15] or simulated over a time domain [16, 17]. The random rough road profiles of classes D and E corresponding to a vehicle speed of 1.5 m/s are depicted over the time domain as shown in Figure 3.

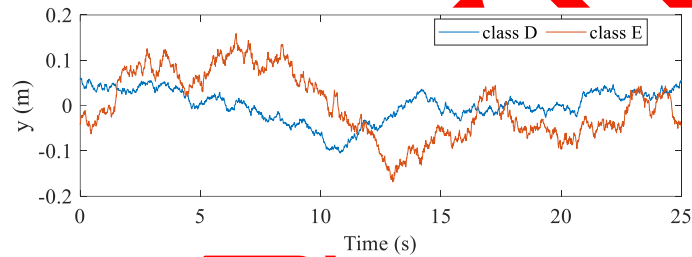


Figure 3. Random road profile at a vehicle speed of 1.5 m/s

Let  $y_0$  denote the amplitude of the road profile,  $\lambda$  represent the wavelength of the road surface,  $\omega = \frac{2\pi v}{\lambda}$  denote the frequency of the oscillation excitation, and  $d$  denote the distance between the axles of the front and rear wheels

$$y_1 = y_0 \sin \omega t; y_2 = y_0 \sin \left( \omega t - \frac{2\pi d}{\lambda} \right) \tag{1}$$

The wind resistance acts on both the vehicle and the object during movement. However, the vehicle's low speed means that the impact of wind resistance on the vehicle is not significant. We are concerned about the impact of wind resistance on the lifted object. If  $A$  ( $m^2$ ) is the cross-sectional area exposed to the wind of the lifted object and  $q_w$  ( $N/m^2$ ) is the wind resistance coefficient, then the wind resistance force  $W$  (N) is determined by the equation:

$$W = Aq_w. \tag{2}$$

### 2.3. Kinetic Energy, Potential Energy and Dissipation Function

The length of segment  $CE$  at any given time is:

$$l_{CE} = \sqrt{l_3^2 + l_4^2 - 2l_3l_4 \cos(\beta - q_5)} \tag{3}$$

The distance from  $D$  to  $CE$  at any given time is:

$$r_{CE} = \frac{l_4 l_5 \sin(\beta - q_5)}{l_{CE}} \quad (4)$$

The static deformation of the cable segment holding the boom is determined from the cable tension through the moment equilibrium equation of the forces acting on the boom with respect to point  $D$  when the boom is in a balanced static state:

$$F_c = \frac{(m_4 g l_3 + m_3 g l_4) \cos(q_{40} + q_{50} + \alpha)}{l_4 l_5 \sin(\beta - q_{50})} \sqrt{l_5^2 + l_4^2 - 2l_4 l_5 \cos(\beta - q_{50})} \quad (5)$$

where  $q_{40}$  and  $q_{50}$  are the initial values of  $q_4$  and  $q_5$ , respectively. The static deformation of the cable segment holding the boom is:

$$\Delta l_i = \frac{F_c}{k_c} \quad (6)$$

The total deformation of the boom support cable is:

$$\Delta l = \Delta l_i + \sqrt{l_5^2 + l_4^2 - 2l_5 l_4 \cos(\beta - q_5)} - \sqrt{l_5^2 + l_4^2 - 2l_5 l_4 \cos(\beta - q_{50})} \quad (7)$$

The kinetic energy of the mechanical system includes the translational kinetic energy along the  $Ox$  and  $Oz$  directions and the rotational kinetic energy about the axis passing through the center of mass of the masses  $m_3$  and  $m_4$ . Let  $v$  (m/s) be the speed of the ASV. The total kinetic energy of the mechanical system is determined by the expression:

$$T = \frac{1}{2} m_1 (v^2 + \dot{q}_1^2) + \frac{1}{2} m_2 (v^2 + \dot{q}_2^2) + \frac{1}{2} m_3 (v^2 + \dot{q}_3^2) + \frac{1}{2} J_c \dot{q}_4^2 + \frac{1}{2} J_b \dot{q}_5^2 + \frac{1}{2} m_4 \left\{ \begin{aligned} &v^2 + l_2^2 \dot{q}_4^2 + l_3^2 (\dot{q}_4 + \dot{q}_5)^2 + \dot{q}_3^2 - 2vl_2 \dot{q}_4 \sin(q_4 + \alpha) - 2vl_3 (\dot{q}_4 + \dot{q}_5) \sin(q_4 + q_5 + \alpha) \\ &+ 2l_2 l_3 \dot{q}_4 (\dot{q}_4 + \dot{q}_5) \cos q_5 + 2\dot{q}_3 l_2 \dot{q}_4 \cos(q_4 + \alpha) + 2\dot{q}_3 l_3 (\dot{q}_4 + \dot{q}_5) \cos(q_4 + q_5 + \alpha) \end{aligned} \right\} + \frac{1}{2} m_5 \left\{ \begin{aligned} &v^2 + \dot{q}_3^2 + l_2^2 \dot{q}_4^2 + l_4^2 (\dot{q}_4 + \dot{q}_5)^2 + l_6^2 (\dot{q}_4 + \dot{q}_5 + \dot{q}_6)^2 - 2vl_2 \dot{q}_4 \sin(q_4 + \alpha) \\ &- 2vl_4 (\dot{q}_4 + \dot{q}_5) \sin(q_4 + q_5 + \alpha) - 2vl_6 (\dot{q}_4 + \dot{q}_5 + \dot{q}_6) \sin(q_4 + q_5 + q_6 + \alpha) \\ &+ 2l_2 l_4 \dot{q}_4 (\dot{q}_4 + \dot{q}_5) \cos q_5 + 2l_2 l_6 (\dot{q}_4 + \dot{q}_5 + \dot{q}_6) \dot{q}_4 \cos(q_5 + q_6) \\ &+ 2l_4 l_6 (\dot{q}_4 + \dot{q}_5 + \dot{q}_6) (\dot{q}_4 + \dot{q}_5) \cos q_6 + 2\dot{q}_3 l_2 \dot{q}_4 \cos(q_4 + \alpha) \\ &+ 2\dot{q}_3 l_4 (\dot{q}_4 + \dot{q}_5) \cos(q_4 + q_5 + \alpha) + 2\dot{q}_3 l_6 (\dot{q}_4 + \dot{q}_5 + \dot{q}_6) \cos(q_4 + q_5 + q_6 + \alpha) \end{aligned} \right\} \quad (8)$$

The total potential energy of the mechanical system is determined by the expression:

$$\begin{aligned} \Pi = & \frac{1}{2}k_t(q_1 - y_1)^2 + \frac{1}{2}k_t(q_2 - y_2)^2 + \frac{1}{2}k_{fs}(q_3 - a_1q_4 - q_1)^2 + \frac{1}{2}k_{rs}(q_3 + a_2q_4 - q_2)^2 \\ & + \frac{1}{2}k_c\Delta l^2 + m_1g(h_1 + q_1) + m_2g(h_2 + q_2) + m_3g(h_3 + q_3) + m_4g \left\{ \begin{aligned} & h_0 + q_3 + l_2 \sin(q_4 + \alpha) \\ & + l_3 \sin(q_4 + q_5 + \alpha) \end{aligned} \right\} \\ & + m_5g \{ h_0 + q_3 + l_2 \sin(q_4 + \alpha) + l_4 \sin(q_4 + q_5 + \alpha) + l_6 \sin(q_4 + q_5 + q_6 + \alpha) \}. \end{aligned} \quad (9)$$

The total dissipated energy of the mechanical system is determined by the expression:

$$\Phi = \frac{1}{2}b_t(\dot{q}_1 - \dot{y}_1)^2 + \frac{1}{2}b_t(\dot{q}_2 - \dot{y}_2)^2 + \frac{1}{2}b_{fs}(\dot{q}_3 - a_1\dot{q}_4 - \dot{q}_1)^2 + \frac{1}{2}b_{rs}(\dot{q}_3 + a_2\dot{q}_4 - \dot{q}_2)^2 + \frac{1}{2}b_c\dot{\Delta}l^2. \quad (10)$$

### 2.3. The System of Differential Equations

Applying the second type of Lagrangian equations to establish the system of differential equations describing the oscillation of the mechanical system, we obtain the following six equations:

$$m_1\ddot{q}_1 + (b_t + b_{fs})\dot{q}_1 - b_{fs}\dot{q}_3 + b_{fs}a_1\dot{q}_4 + (k_t + k_{fs})q_1 - k_{fs}q_3 + k_{fs}a_1q_4 + m_1g = k_t y_1 + b_t \dot{y}_1 \quad (11)$$

$$m_2\ddot{q}_2 + (b_t + b_{rs})\dot{q}_2 - b_{rs}\dot{q}_3 - b_{rs}a_2\dot{q}_4 + (k_t + k_{rs})q_2 - k_{rs}q_3 - k_{rs}a_2q_4 + m_2g = k_t y_2 + b_t \dot{y}_2 \quad (12)$$

$$\begin{aligned} & (m_3 + m_4 + m_5)\ddot{q}_3 + \left\{ \begin{aligned} & (m_4l_3 + m_5l_4)\cos(q_4 + q_5 + \alpha) \\ & + m_5l_6\cos(q_4 + q_5 + q_6 + \alpha) \end{aligned} \right\} \ddot{q}_5 + m_5l_6\cos(q_4 + q_5 + q_6 + \alpha)\ddot{q}_6 \\ & + \{ (m_4 + m_5)l_2\cos(q_4 + \alpha) + (m_4l_3 + m_5l_4)\cos(q_4 + q_5 + \alpha) + m_5l_6\cos(q_4 + q_5 + q_6 + \alpha) \} \ddot{q}_4 \\ & - b_{fs}\dot{q}_1 - b_{rs}\dot{q}_2 + (b_{fs} + b_{rs})\dot{q}_3 - (b_{fs}a_1 - b_{rs}a_2)\dot{q}_4 - (m_4 + m_5)l_2\dot{q}_4^2\sin(q_4 + \alpha) \\ & - (m_4l_3 + m_5l_4)(\dot{q}_4 + \dot{q}_5)^2\sin(q_4 + q_5 + \alpha) - m_5l_6(\dot{q}_4 + \dot{q}_5 + \dot{q}_6)^2\sin(q_4 + q_5 + q_6 + \alpha) \\ & - k_{fs}q_1 - k_{rs}q_2 + (k_{fs} + k_{rs})q_3 - (k_{fs}a_1 - k_{rs}a_2)q_4 + (m_3 + m_4 + m_5)g = 0 \end{aligned} \quad (13)$$

$$\begin{aligned} & \left\{ \begin{aligned} & m_4l_3\cos(q_4 + q_5 + \alpha) + m_4l_2\cos(q_4 + \alpha) + m_5l_2\cos(q_4 + \alpha) \\ & + m_5l_6\cos(q_4 + q_5 + q_6 + \alpha) + m_5l_4\cos(q_4 + q_5 + \alpha) \end{aligned} \right\} \ddot{q}_3 \\ & + \left\{ \begin{aligned} & J_c + m_4l_2^2 + m_4l_3^2 + 2m_4l_2l_3 + m_5l_2^2 + m_5l_4^2 + 2m_5l_2l_4\cos q_5 \\ & + m_5l_6^2 + 2m_5l_2l_6\cos(q_5 + q_6) + 2m_5l_4l_6\cos q_6 \end{aligned} \right\} \ddot{q}_4 \\ & + \{ m_4l_3^2 + m_4l_2l_3\cos q_5 + m_5l_4^2 + m_5l_2l_4\cos q_5 + m_5l_6^2 + m_5l_2l_6\cos(q_5 + q_6) + 2m_5l_4l_6\cos q_6 \} \ddot{q}_5 \\ & + (m_5l_6^2 + m_5l_2l_6\cos(q_5 + q_6) + m_5l_4l_6\cos q_6)\ddot{q}_6 + a_1b_{fs}\dot{q}_1 - a_2b_{rs}\dot{q}_2 - (a_1b_{fs} - a_2b_{rs})\dot{q}_3 \\ & + (b_{fs}a_1^2 + b_{rs}a_2^2)\dot{q}_4 + a_1k_{fs}q_1 - a_2k_{rs}q_2 + (-a_1k_{fs} + a_2k_{rs})q_3 + (a_1^2k_{fs} + a_2^2k_{rs})q_4 \\ & + m_4gl_2\cos(q_4 + \alpha) + m_4gl_3\cos(q_4 + q_5 + \alpha) + m_5gl_2\cos(q_4 + \alpha) + m_5gl_4\cos(q_4 + q_5 + \alpha) \\ & + m_5gl_6\cos(q_4 + q_5 + q_6 + \alpha) - m_5l_2l_6(\dot{q}_6 + 2\dot{q}_4 + \dot{q}_5)(\dot{q}_5 + \dot{q}_6)\sin(q_5 + q_6) \\ & - m_5l_4l_6(2\dot{q}_4 + 2\dot{q}_5 + \dot{q}_6)\sin q_6\dot{q}_6 - (m_4l_2l_3 + m_5l_2l_4)(2\dot{q}_4 + \dot{q}_5)\sin q_5\dot{q}_5 \\ & = -Wl_2\sin(q_4 + \alpha) - Wl_4\sin(q_4 + q_5 + \alpha) - Wl_6\sin(q_4 + q_5 + q_6 + \alpha) \end{aligned} \quad (14)$$

$$\begin{aligned}
 & m_5 l_6 \cos(q_4 + q_5 + q_6 + \alpha) \ddot{q}_3 + \{m_3 l_6^2 + m_5 l_2 l_6 \cos(q_5 + q_6) + m_5 l_4 l_6 \cos q_6\} \ddot{q}_4 \\
 & + (m_5 l_6^2 + m_5 l_4 l_6 \cos q_6) \ddot{q}_5 + m_5 l_6^2 \ddot{q}_6 + m_5 \{l_2 l_6 \dot{q}_4^2 \sin(q_5 + q_6) + l_4 l_6 (\dot{q}_4 + \dot{q}_5)^2 \sin q_6\} \\
 & + m_5 g l_6 \cos(q_4 + q_5 + q_6 + \alpha) = -W l_6 \sin(q_4 + q_5 + q_6 + \alpha)
 \end{aligned} \tag{15}$$

$$\begin{aligned}
 & \{m_4 l_3 \cos(q_4 + q_5 + \alpha) + m_5 l_4 \cos(q_4 + q_5 + \alpha) + m_5 l_6 \cos(q_4 + q_5 + q_6 + \alpha)\} \ddot{q}_3 \\
 & + \{(m_4 l_3^2 + m_5 l_4^2) + (m_4 l_2 l_3 + m_5 l_2 l_4) \cos q_5 + m_5 l_6^2 + m_5 l_2 l_6 \cos(q_5 + q_6) + 2m_5 l_4 l_6 \cos q_6\} \ddot{q}_4 \\
 & + \{(m_4 l_3^2 + m_5 l_4^2) + J_b + m_5 l_6^2 + 2m_5 l_4 l_6 \cos q_6\} \ddot{q}_5 + (m_5 l_6^2 + m_5 l_4 l_6 \cos q_6) \ddot{q}_6 \\
 & + \{m_4 l_2 l_3 \sin q_5 + m_5 (l_2 l_4 \sin q_5 + l_2 l_6 \sin(q_5 + q_6))\} \dot{q}_4^2 - m_5 l_4 l_6 (2\dot{q}_4 + 2\dot{q}_5 + \dot{q}_6) \dot{q}_6 \sin q_6 \\
 & + m_4 g l_3 \cos(q_4 + q_5 + \alpha) + m_5 g l_4 \cos(q_4 + q_5 + \alpha) + m_5 g l_6 \cos(q_4 + q_5 + q_6 + \alpha) \\
 & - k_c \Delta l \frac{l_5 l_4 \sin(\beta - q_5)}{\sqrt{l_5^2 + l_4^2 - 2l_5 l_4 \cos(\beta - q_5)}} + b_c \dot{\Delta l} \frac{-l_5 l_4 \sin(\beta - q_5)}{\sqrt{l_5^2 + l_4^2 - 2l_5 l_4 \cos(\beta - q_5)}} \\
 & = -W l_4 \sin(q_4 + q_5 + \alpha_1) - W l_6 \sin(q_4 + q_5 + q_6 + \alpha_1).
 \end{aligned} \tag{16}$$

In Equation (16), component  $\dot{\Delta l}$  is determined as follows:

$$\dot{\Delta l} = \frac{-l_5 l_4 \sin(\beta - q_5) \dot{q}_5}{\sqrt{l_5^2 + l_4^2 - 2l_5 l_4 \cos(\alpha_3 - q_5)}}. \tag{17}$$

The input parameters for solving the system are provided in Table 1 below [18]. The technical parameters related to the base vehicle in Table 1 are the parameters of the BRDM-2 vehicle. The system of differential equations can be represented in matrix form and solved using simulation methods in MATLAB with the initial conditions as follows:

$$\text{Initial displacement: } [q_{10} \ q_{20} \ q_{30} \ q_{40} \ q_{50} \ q_{60}]^T = [0 \ 0 \ 0 \ 0 \ 0.25\pi \ 1.194\pi]^T$$

$$\text{Initial velocity: } [\dot{q}_{10} \ \dot{q}_{20} \ \dot{q}_{30} \ \dot{q}_{40} \ \dot{q}_{50} \ \dot{q}_{60}]^T = [0 \ 0 \ 0 \ 0 \ 0 \ 0]^T.$$

**Table 1.** The input parameters.

Parameter	Value	Parameter	Value	Parameter	Value
$k_t$ (N/m)	$8 \times 10^5$	$J_c$ (kgm <sup>2</sup> )	125	$l_2$ (m)	2.5
$k_{fs}$ (N/m)	$195 \times 10^3$	$m_1$ (kg)	305	$l_3$ (m)	2.5
$k_{rs}$ (N/m)	$295 \times 10^3$	$m_2$ (kg)	300	$l_4$ (m)	5.0
$k_c$ (N/m)	$2 \times 10^6$	$m_3$ (kg)	5450	$l_5$ (m)	4.6
$b_t$ (N.s/m)	500	$m_4$ (kg)	80	$l_6$ (m)	2.0
$b_{fs}$ (N.s/m)	24000	$m_5$ (kg)	500	$A$ (m <sup>2</sup> )	0.5
$b_{rs}$ (N.s/m)	24000	$a_1$ (m)	1.8	$q_w$ (N/m <sup>2</sup> )	250
$b_c$ (N.s/m)	500	$a_2$ (m)	2.4	$\alpha$ (rad)	$\pi/18$
$J_b$ (kgm <sup>2</sup> )	3250	$l_1$ (m)	2.2	$\beta$ (rad)	$125 \times \pi/180$

The uneven road surface can induce various types of oscillations in an ASV, affecting its comfort, safety, and lifespan, especially the oscillations of the object. We consider the impact of several typical rough road

surfaces on the oscillations of the vehicle chassis, boom, and object during vehicle movement at speeds of 1 m/s, 1.5 m/s, and 2 m/s.

### 3. RESULTS AND DISCUSSION

#### 3.1. The Influence of a Sinusoidal Rough Road Surface

The sinusoidal rough road surface (SRRS) is an idealized road profile often used in theoretical and simulation studies. Considering the case of a vehicle moving on a sinusoidal rough road surface with an amplitude of 15 cm and a wavelength of 8 m. The graphs in Figure 4 show the oscillations of the object and the boom corresponding to the vehicle's speeds. From the graph in Figure 4a, we observe that as the vehicle speed increases, the amplitude of the object's oscillation also increases. The maximum amplitudes of  $q_6$  corresponding to speeds of 1 m/s, 1.5 m/s, and 2 m/s are 0.2 rad, 0.3 rad, and 0.46 rad, respectively. It is noteworthy that when the speed reaches 2 m/s, the maximum amplitude of  $q_6$  jumps significantly. Regarding the oscillation of the boom, the graph in Figure 4b shows that during the vehicle's movement, the cable holding the boom remains taut, and the boom only oscillates around its equilibrium position with a very small amplitude. The maximum amplitude of the boom's oscillation also increases as the vehicle speed increases. This is consistent with the oscillation of the object.

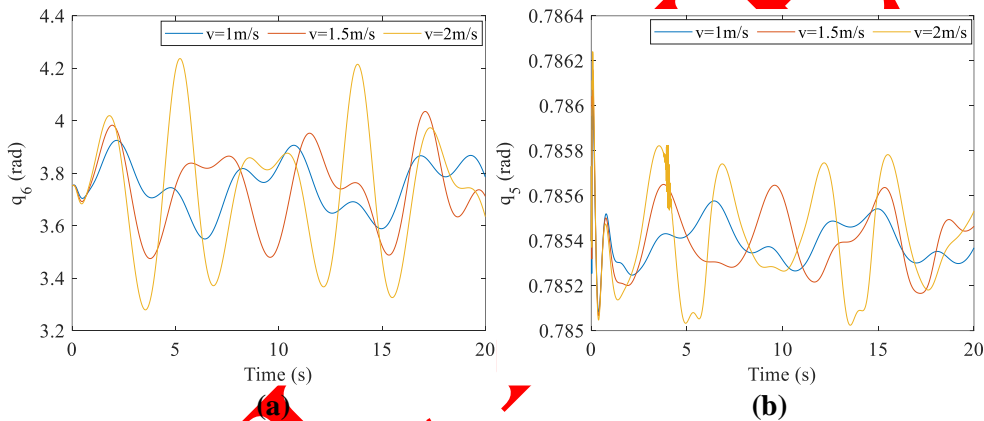


Figure 4. Oscillation of the object and the boom on the SRRS; a) object b) boom

The graphs in Figure 5 show the oscillation of the vehicle chassis when moving on the sinusoidal rough road surface.

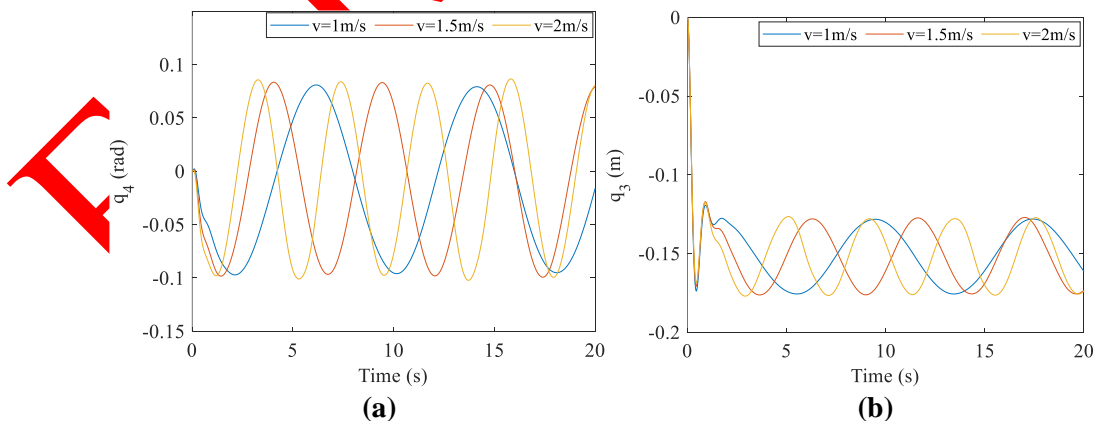


Figure 5. Oscillation of the chassis on a SRRS; a) roll angle b) vertical displacement

We observe that the oscillation patterns of  $q_3$  and  $q_4$  also have sinusoidal shapes, with longer periods corresponding to lower speeds. When the road roughness remains constant, the amplitudes of the vertical displacement and the roll angle of the chassis are approximately equal. At the equilibrium position, the

center of gravity of the chassis is lowered by about 15 cm compared to its initial position, and the approximate roll angle amplitude of the chassis is 0.09 rad.

### 3.2. The Influence of Randomly Rough Road Surfaces of Class D

The randomly rough road surface (RRRS) of class D and E, as defined by ISO 8608, represents poor road conditions commonly encountered in reality. They remain a standardized model and may not fully capture the complexity of real-world road surfaces. However, in many studies on vehicle dynamics, describing the road surface according to this standard is the closest to reality in theoretical studies. The oscillation of the object when the vehicle moves on the RRRS of class D is depicted in Figure 6. From the graph in Figure 6a, we observe that the oscillation amplitude of  $q_6$  increases over time for each different speed, and the amplitude is larger when the vehicle's speed is higher. This is understood as the vehicle moving at a constant speed, the amplitude of the object gradually increases with the distance traveled. Comparing between speeds, we find that the amplitude of  $q_6$  reaches approximately 0.12 rad after 18s of movement at a speed of  $v = 1$  m/s, after 10s of movement at a speed of  $v = 1.5$  m/s, and after 5s of movement at a speed of  $v = 2$  m/s. The angular velocity  $\dot{q}_6$  shown in Figure 6b also exhibits an increasing trend over time, meaning that the object oscillates faster as it moves. Considering the overall oscillation of the heavy object when the vehicle moves on a RRRS of class D, we can make the general observation that the vehicle's speed affects the oscillation of the object. For speeds of 1 m/s and 1.5 m/s, the difference is not very pronounced, but when the speed increases to 2 m/s, the oscillation amplitude of the object is significantly larger compared to the other cases.

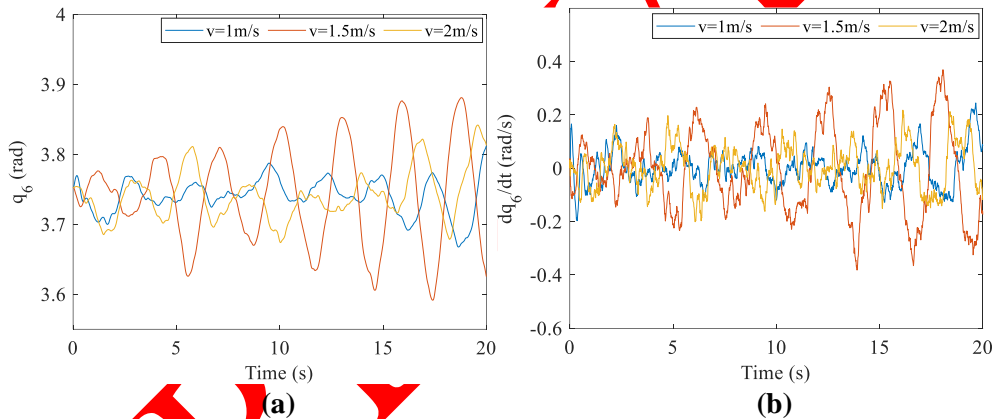


Figure 6. Oscillation of the object on RRRS of class D; a) displacement b) angular velocity

The results of the oscillation survey of the boom are depicted in Figure 7. For different vehicle speeds, the boom oscillates around its equilibrium position with a very small angular amplitude, and there is no specific pattern. This result is entirely consistent with the case of boom oscillation when the vehicle moves on a RRRS.

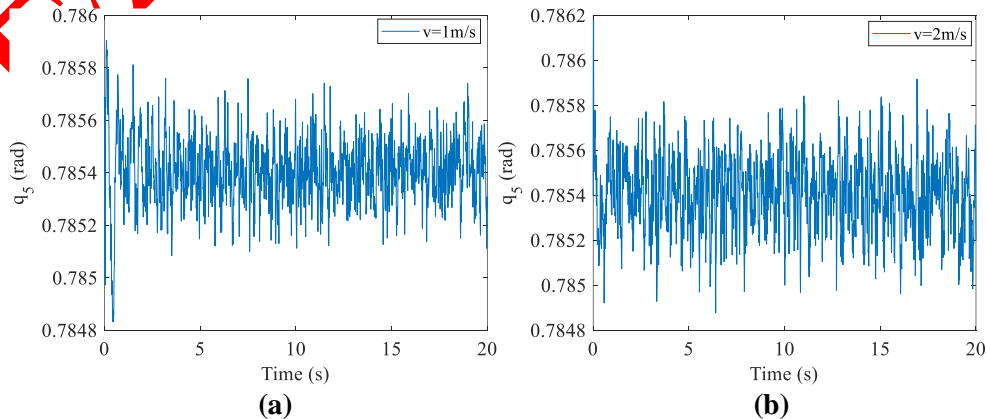
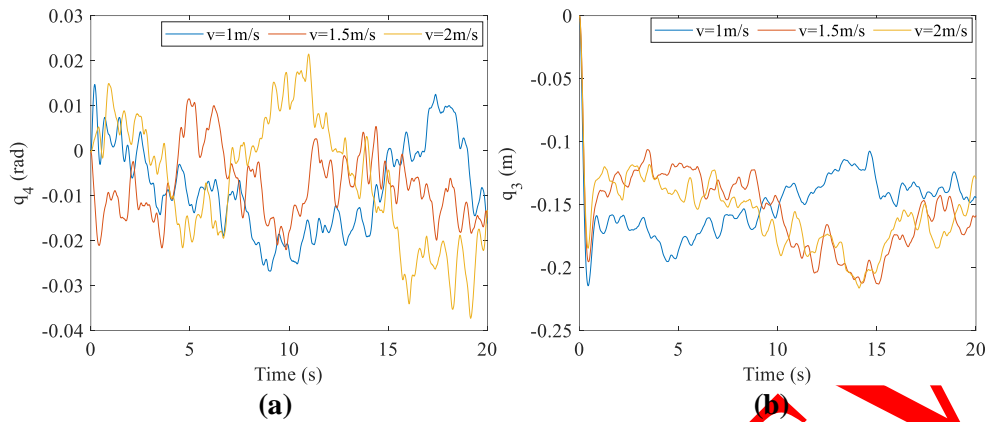


Figure 7. Oscillation of the boom on RRRS of class D; a)  $v = 1$  m/s b)  $v = 2$  m/s

The oscillation of the vehicle chassis, including the roll angle  $q_4$  and the vertical displacement  $q_3$ , is shown in Figure 8.



**Figure 8.** Oscillation of the chassis on RRRS of class D; a) roll angle b) vertical displacement

The chassis oscillation takes on a random form depending on the randomness of the class D road surface profile and aligns well with the convex and concave features of the road surface. The maximum roll angle amplitude of the chassis reaches approximately 0.035 rad, while the lowest position of the chassis center of gravity is about 22 cm lower than the initial position. This is related to the vehicle's suspension characteristics, indicating that the vehicle can both hold the object and traverse rough terrain of class D.

### 3.3. The Influence of Randomly Rough Road Surfaces of Class E

The oscillation of the object and the boom when the vehicle moves on a RRRS in class E are shown in Figure 9. We observe that the patterns of  $q_5$  and  $q_6$  are similar to the cases examined above. The amplitude of  $q_6$  also increases with the distance traveled by the vehicle and has a larger maximum value for higher speeds. The oscillation of the boom corresponding to speeds of 1 m/s, 1.5 m/s, and 2 m/s all exhibit random patterns with relatively small maximum amplitudes. The graph in Figure 9b illustrates the oscillation of the boom corresponding to a speed of  $v = 1$  m/s.

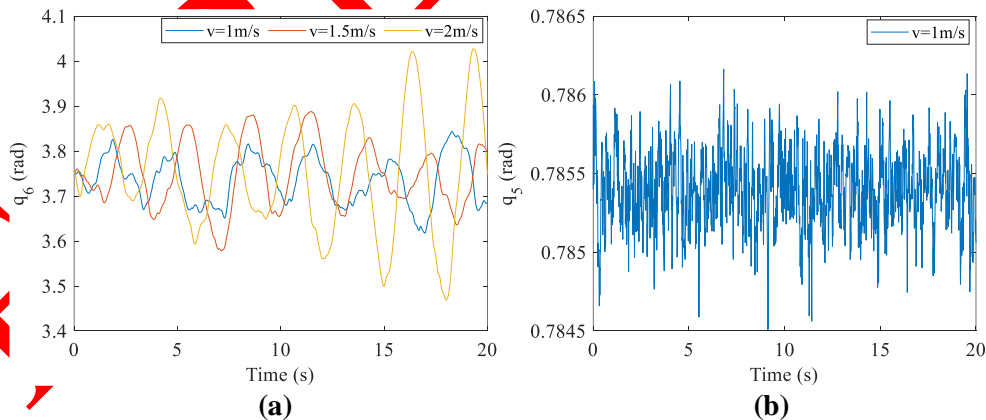


**Figure 9.** Oscillation of the object and the boom on RRRS of class E; a) oscillation of the object b) oscillation of the boom

The oscillation of the vehicle chassis is depicted in Figure 10, and the oscillation patterns of  $q_3$  and  $q_4$  also exhibit random forms corresponding to the terrain. The maximum roll angle amplitude of the chassis reaches approximately 0.06 rad, and the lowest position of the chassis center of gravity compared to the initial position is about 26 cm.

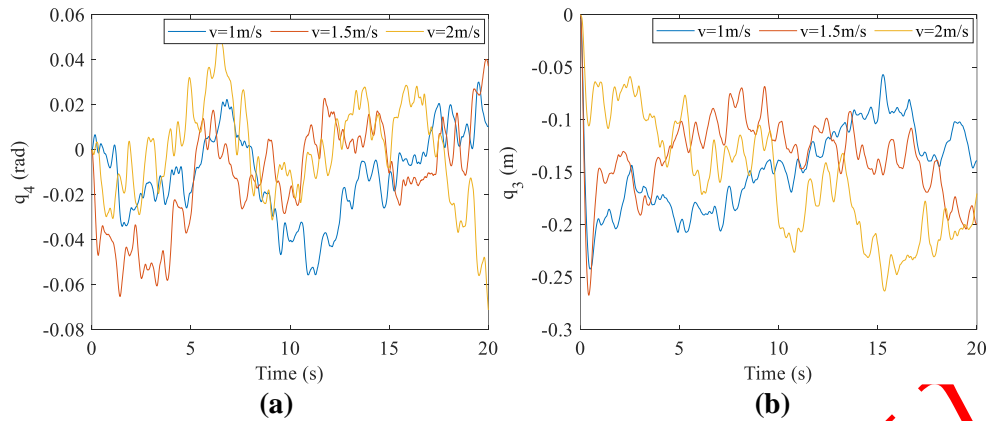


**Figure 10.** Oscillation of the chassis on RRRS of class E; a) roll angle b) vertical displacement

From the three cases examined above, we focus more on the oscillation of the object and the boom because the research results show that the off-road capability of the vehicle chassis fully meets the requirements for various types of rough terrain in classes D and E. Comparing the oscillation characteristics of  $q_6$  in all three terrain cases mentioned above, we observe the most pronounced common feature: the oscillation amplitude increases as the vehicle speed increases, and its maximum value gradually increases over time. Minimizing the oscillation of the object during vehicle movement is a crucial factor in evaluating the vehicle's performance when used as a mobile crane. This is the next objective that needs to be studied in greater depth.

#### 4. CONCLUSION

The study has developed a dynamic model of an ASV simultaneously holding and moving objects on a randomly or sinusoidally rough road. This research model is unique in its combination of vehicle motion and crane operation. The paper's results demonstrate the appropriate interaction between the oscillation of the vehicle chassis and the road surface during movement. As the vehicle speed increases from 1 m/s to 2 m/s, the object oscillates around the vertical axis, and the angle amplitude increases. This oscillation highlights the need to minimize the oscillation amplitude of the object. This study holds significant importance in the military sector by considering the impact of working conditions on the movement of ASVs and aiming to evaluate their operational capabilities and versatility as mobile cranes. The paper's results provide theoretical groundwork for improving a range of original Soviet-made armored personnel carriers, which are currently in use in many economically developing countries.

#### ACKNOWLEDGEMENT

The authors would like to thank the Le Quy Don Technical University for giving us the opportunity to conduct this research. This paper is the result of the research project with code 24.1.74.

#### CONFLICTS OF INTEREST

No conflict of interest was declared by the authors.

#### REFERENCES

- [1] Boreiry, M., Ebrahimi-Nejad, S., and Marzbanrad, J., "Sensitivity analysis of chaotic vibrations of a full vehicle model with magnetorheological damper", *Chaos, Solitons and Fractals*, 127: 428–442, (2019).
- [2] Zhu, Q., Ishitobi, M., "Chaotic vibration of a nonlinear full-vehicle model. *International Journal of Solids and Structures*", 43(3–4): 747–759, (2006).

- [3] Yang, J., Dong, M., "Research on Vibration of Automobile Suspension Design", MATEC Web of Conferences, 153: 04008, (2018).
- [4] Park, D.W., Papagiannakis, A.T., and Kim, I.T., "Analysis of dynamic vehicle loads using vehicle pavement interaction model", KSCE Journal of Civil Engineering, 18(7): 2085-2092, (2014).
- [5] Demic, M., Sakota, Z.B., and Miloradović, D.M., "Impact of truck's power train layout on driver's fore-and-aft vibration loads", Journal of Mechanical Engineering and Modern Technology, 1(1): 37-51, (2018).
- [6] Davis, L.E, Bunker, J.M., "Dynamic load sharing for heavy vehicles : a new metric", Road and Transport Research, 18(4): 23-37, (2009).
- [7] Zhang, J., Deng, Y., Zhang, N., and Zhang, B., "Vibration performance analysis of a mining vehicle with bounce and pitch tuned hydraulically interconnected suspension", Chinese Journal of Mechanical Engineering, 32: 5, (2019).
- [8] Attia, T., Vamvoudakis, K.G., Kochersberger, K., Bird, J., and Furukawa, T., "Simultaneous dynamic system estimation and optimal control of vehicle active suspension", Vehicle System Dynamics, 57(10): 1467–1493, (2019).
- [9] Aljarbough, A., Fayaz, M., Qureshi, M.S., and Boujoudar, Y., "Hybrid sliding mode control of full-car semi-active suspension systems", Symmetry, 13(12): 2442, (2021).
- [10] Tian, M., Nguyen, V., "Control performance of suspension system of cars with PID control based on 3D dynamic model", Journal of mechanical engineering, automation and control systems, 1(1): 1-10, (2020).
- [11] Zhao, L., Zhou, C., Yu, Y., and Yang, F., "A method to evaluate stiffness and damping parameters of cabin suspension system for heavy truck", Advances in Mechanical Engineering, 8(7): 1-9, (2016).
- [12] Basaran, S., Basaran, M., "Vibration control of truck cabins with the adaptive vectorial backstepping design of electromagnetic active suspension system", IEEE Access, 8:173056-173067, (2020).
- [13] Agostinacchio, M., Ciampa, D., and Olita, S., "The vibrations induced by surface irregularities in road pavements – a Matlab® approach", European Transport Research Review, 6: 267–275, (2014).
- [14] Cao, D.J., Lin, C., Sun, F., and Chang, H., "Simulation of road roughness based on using IFFT method", 2012 Third World Congress on Software Engineering, Wuhan, China, 190-193, (2012).
- [15] Zhang, Y., Zhao, H., and Lie, S.T., "A simple approach for simulating the road surface roughness involved in vehicle-bridge interaction systems", International Journal of Structural Stability and Dynamics, 18(7): 1871009, (2018).
- [16] Tuan, N.V., Quynh, L.V., Thao, V.T.P., and Duy, L.Q., "Optimal design parameters of air suspension systems for semi-trailer truck. Part 1: modeling and algorithm", Vibroengineering PROCEDIA, 33: 72–77, (2020).
- [17] Long, L.X., Quynh, L.V., and Cuong, B.V., "Study on the influence of bus suspension parameters on ride comfort", Vibroengineering PROCEDIA, 21: 77–82, (2018).
- [18] Duong, L.V., Tuan, L.A., "Modeling and observer-based robust controllers for telescopic truck cranes", Mechanism and Machine Theory, 173: 104869, (2022).

- [19] Mijailović, R., "Modelling the dynamic behaviour of the truck-crane", *Transport*, 26(4): 410–417, (2011).
- [20] Cekus, D., Kwiatóń, P., "Effect of the rope system deformation on the working cycle of the mobile crane during interaction of wind pressure", *Mechanism and Machine Theory*, 153: 104011, (2020).
- [21] Tuan, L.A., Lee, S.G., "Modeling and advanced sliding mode controls of crawler cranes considering wire rope elasticity and complicated operations", *Mechanical Systems and Signal Processing*, 103: 250–263, (2017).
- [22] Tuan, L.A., "Fractional-order fast terminal back-stepping sliding mode control of crawler cranes", *Mechanism and Machine Theory*, 137: 297–314, (2019).
- [23] Hieu, N.Q., Hong, K.S., "Adaptive sliding mode control of container cranes", *IET Control Theory & Applications*, 6 (5): 662–668, (2012).
- [24] Tuan, L.A., Lee, S.G., Nho, L.C., and Cuong, H.M., "Robust controls for ship-mounted container cranes with viscoelastic foundation and flexible hoisting cable", *Proceedings of the Institution of Mechanical Engineers, Part I: Journal of Systems and Control Engineering*, 229(7): 662–674, (2015).
- [25] Wu, T.S., Karkouba, M., Yu, W.S., Chen, C.T., Her, M.G., and Wu, K.W., "Anti-sway tracking control of tower cranes with delayed uncertainty using a robust adaptive fuzzy control", *Fuzzy Sets and Systems*, 290: 118–137, (2016).
- [26] Chen, H., Fang, Y., and Sun, N., "An adaptive tracking control method with swing suppression for 4-DOF tower crane systems", *Mechanical Systems and Signal Processing*, 123: 426–442, (2019).
- [27] Vaughan, J., Kim, D., and Singhose, W., "Control of tower cranes with double-pendulum payload dynamics", *IEEE Transactions on Control Systems Technology*, 18(6): 1345-1358, (2010).
- [28] Fasih, S.M., Mohamed, Z., Husain, A.R., Ranli, L., Abdullahi, A.M., and Anjum, W., "Payload swing control of a tower crane using a neural network-based input shaper", *Measurement and Control*, 53(7-8): 1171–1182, (2020).
- [29] Nishimoto, R., Kikuuwe, R., "Position-commanding anti-sway controller for 2-D overhead cranes under velocity and acceleration constraints", *IEEE Access*, 11: 35069-35079, (2023).
- [30] Liu, H., Cheng, W., and Li, Y., "Dynamic responses of an overhead crane's beam subjected to a moving trolley with a pendulum payload", *Shock and Vibration*, 2019(6): 1-14, (2019).